

# Reclassify High-Grade Serous Ovarian Cancer Patients Into Different Molecular Subtypes With Discrepancy Prognoses and Therapeutic Responses Based on Cancer-Associated Fibroblast-Enriched Prognostic Genes

Biomedical Engineering and  
Computational Biology  
Volume 15: 1–13  
© The Author(s) 2024  
Article reuse guidelines:  
sagepub.com/journals-permissions  
DOI: 10.1177/11795972241274024



Xiangxiang Liu<sup>1\*</sup>, Guoqiang Ping<sup>2\*</sup>, Dongze Ji<sup>2</sup>, Zhifa Wen<sup>1</sup>  
and Yajun Chen<sup>1</sup>

<sup>1</sup>Department of Clinical Laboratory, Women's Hospital of Nanjing Medical University, Nanjing Women and Children's Healthcare Hospital, Nanjing, Jiangsu, China. <sup>2</sup>Department of Pathology, the First Affiliated Hospital of Nanjing Medical University, Nanjing, Jiangsu, China.

**ABSTRACT:** Cancer-associated fibroblasts (CAFs) play critical roles in the metastasis and therapeutic response of high-grade serous ovarian cancer (HGSC). Our study intended to select HGSC patients with unfavorable prognoses and therapeutic responses based on CAF-enriched prognostic genes. The bulk RNA and single-cell RNA sequencing (scRNA-seq) data of tumor tissues were collected from the TCGA and GEO databases. The infiltrated levels of immune and stromal cells were estimated by multiple immune deconvolution algorithms and verified through immunohistochemical analysis. The univariate Cox regression analyses were used to identify prognostic genes. Gene Set Enrichment Analysis (GSEA) was conducted to annotate enriched gene sets. The Genomics of Drug Sensitivity in Cancer (GDSC) database was used to explore potential alternative drugs. We found the infiltrated levels of CAFs were remarkably elevated in advanced and metastatic HGSC tissues and identified hundreds of genes specifically enriched in CAFs. Then we selected 6 CAF-enriched prognostic genes based on which HGSC patients were reclassified into 2 subclusters with discrepancy prognoses. Further analysis revealed that the HGSC patients in cluster-2 tended to undergo poor responses to traditional chemotherapy and immunotherapy. Subsequently, we selected 24 novel potential therapeutic drugs for cluster-2 HGSC patients. Moreover, we discovered a positive correlation of infiltrated levels between CAFs and monocytes/macrophages in HGSC tissues. Collectively, our study successfully reclassified HGSC patients into 2 different subgroups that have discrepancy prognoses and responses to current therapeutic methods.

**KEYWORDS:** Ovarian cancer, cancer-associated fibroblast, immunity, prognosis, therapy

**RECEIVED:** December 14, 2023. **ACCEPTED:** July 2, 2024.

**TYPE:** Original Research

**FUNDING:** The author(s) received no financial support for the research, authorship, and/or publication of this article.

**DECLARATION OF CONFLICTING INTERESTS:** The author(s) declared no potential conflicts of interest with respect to the research, authorship, and/or publication of this article.

**CORRESPONDING AUTHORS:** Yajun Chen, Department of Clinical Laboratory, Women's Hospital of Nanjing Medical University, Nanjing Women and Children's Healthcare Hospital, No. 123, Tianfei Lane, Mochou Road, Qinhuai District, Nanjing, Jiangsu 210004, China. Email: Yajunchen\_doctor@163.com

Zhifa Wen, Department of Clinical Laboratory, Women's Hospital of Nanjing Medical University, Nanjing Women and Children's Healthcare Hospital, No. 123, Tianfei Lane, Mochou Road, Qinhuai District, Nanjing, Jiangsu 210004, China. Email: zhifa.wen@njmu.edu.cn

## Introduction

High-grade serous ovarian carcinoma (HGSC) accounts for approximately 70% of ovarian cancer (OC) which ranks the highest mortality rate among gynecological malignancies.<sup>1,2</sup> Deep in the pelvic cavity, ovarian lesions are often without specific clinical symptoms in the early stage. Whereas when symptoms appear, 70% of tumors are already in the late stage with peritoneal metastasis.<sup>3,4</sup> Although the therapeutic methods develop, the overall survival of metastatic HGSC patients remains poor due to the acquired drug resistance and release.<sup>5</sup> Therefore, it is necessary to search for novel therapeutic strategies for HGSC patients.

Cancer cells live in a complex tumor microenvironment (TME) containing stromal cells, immune cells, and extracellular matrix (ECM).<sup>6</sup> Cancer-associated fibroblasts (CAFs), a critical component of TME, are significantly associated with the malignancy progression of OC.<sup>7</sup> For example, CAFs release SLPI (Secretory Leukocyte Peptidase Inhibitor) protein to promote

OC metastasis via activating the PI3K/AKT signaling pathway.<sup>8</sup> Emerging evidence has proved that CAFs can shape an immunosuppressive TME by increasing the proportions of immunosuppressive cells and restricting the recruitment of immune effector cells that enable cancer cells to evade immune surveillance.<sup>9</sup> For example, CAFs promote M2 polarization of macrophages to enhance pancreatic tumor progression.<sup>10</sup> CAFs are also associated with the therapeutic response of OC, such as resistance to platinum and anti-angiogenic drugs.<sup>11–13</sup> Recently, emerging studies have deciphered the implications of CAFs on clinical outcome prediction of OC patients.<sup>14</sup> However, it remained unclear whether CAF-enriched genes can be directly implemented to select OC patients who may undergo unfavorable prognoses and be resistant to current therapeutic methods.

In this study, we successfully reclassified HGSC patients into different subgroups with distinct prognoses and discrepancy responses to traditional chemotherapy and immunotherapy based on CAF-enriched genes. Besides, we successfully selected twenty-four drug compounds as the potential alternative to traditional treatment of HGSC patients and verified the

\*These authors contributed equally to this work.



Creative Commons Non Commercial CC BY-NC: This article is distributed under the terms of the Creative Commons Attribution-NonCommercial 4.0 License (<https://creativecommons.org/licenses/by-nc/4.0/>) which permits non-commercial use, reproduction and distribution of the work without further permission provided the original work is attributed as specified on the SAGE and Open Access pages (<https://us.sagepub.com/en-us/nam/open-access-at-sage>).

**Table 1.** The information on the demographics of patients in the datasets.

TCGA		GSE26193		GSE30161		
AGE	59.47 ± 11.39	AGE	/	AGE	62.57 ± 10.61	
FIGO stage		FIGO stage		FIGO stage		
I	1	I	12	I	0	
II	21	II	5	II	0	
III	286	III	48	III	50	
IV	54	IV	14	IV	5	
Grade		Grade		Grade		
G1	1	G1	4	unknown	4	
G2	42	G2	19	well	2	
G3	318	G3	56	moderate	19	
G4	1	G4	0	poor	30	
Therapeutic drug						
Carboplatin						2
Carboplatin/Cytoxan						1
Carboplatin/Taxol						46
Cisplatin/Cytoxan						1
Cisplatin/Taxol						5

cooperative relationship between CAFs and macrophages in HGSC progression.

## Materials and Methods

### Bulk RNA-seq data analysis

The RNA sequencing data of HGSC tissues were obtained from the TCGA OC cohort (<https://portal.gdc.cancer.gov>) and Three GEO datasets (GSE133296, GSE26193, and GSE30161).<sup>15-17</sup> The expression values of each gene were normalized. The R “limma” package was used to identify differentially expressed genes (DEGs) based on a criterion of  $|\log_2FC| \geq 1$  and  $P < .05$ . The GSE133296 dataset consisted of 10 primary HGSC tissues and 20 metastatic HGSC tissues (omental and intraperitoneal metastasis). The GSE30161 dataset included 23 chemotherapy-resistant serous OC tissues and 33 chemotherapy-sensitive serous OC tissues, and the GSE26193 dataset included 107 HGSC patients with follow-up times. Lastly, the TCGA HGSC cohort included 303 patients with exact overall survival times regardless of the TP53 mutation status. The information on the demographics of patients in the datasets was listed in Table 1.

### scRNA-seq data analysis

The scRNA-sequencing data of metastatic HGSC tissues deposited in the GSE151214 dataset<sup>18</sup> were analyzed by the

Tumor Immune Single-cell Hub (TISCH) database (<http://tisch.comp-genomics.org/home/>).<sup>19</sup> The GSE151214 dataset contains 59 446 cells from 8 HGSC tissues and was sequenced using the 10× Genomics platform. The single-cell level expression matrix values were normalized via the “Seurat” package to scale the raw counts in each cell to 10 000. Quality control, cell clustering, and type annotation were performed using the MAESTRO algorithm.

### Functional enrichment analysis

The biological process (BP), molecular function (MF), and cellular component (CC) categories of Gene Ontology (GO) analysis were conducted in the DAVID database (<https://david.ncifcrf.gov>). The results were visualized using OmicShare (<http://www.omicshare.com/tools>). In addition, GSEA analysis was performed based on the MSigDB database (<http://www.gsea-msigdb.org/gsea/msigdb/index.jsp>). The significantly enriched gene sets were selected with criteria of  $|NES| > 1$ , NOM  $P$ -value  $< .05$ , and FDR value  $< 0.25$ . Enrichment analysis was conducted using GSEA 4.3.0 software.

### Evaluating the infiltrated levels of CAFs and immune cells

We used the TIMER2 website (<http://timer.cistrome.org>) to estimate the infiltrated levels of stromal and immune cells in

ovarian carcinoma tissues using multiple immune deconvolution methods, including the MCPOUNTER, EPIC, and XCELL algorithms.

### Immunohistochemistry (IHC)

Xylene and alcohol were first used to deparaffinize HGSC tissue sections (2  $\mu$ m thick). Then antigen retrieval was completed by using sodium citrate buffer (pH 6.0). Next, tissue sections were incubated with mouse monoclonal antibody to  $\alpha$ -SMA (1:200, ab7817, Abcam, USA) and rabbit monoclonal antibody to CD68 (1:100, ab283654, Abcam, USA) overnight at 4°C. Subsequently, sections were washed with PBS thrice and further incubated with corresponding biotin-labeled secondary antibodies for 40 minutes at room temperature. Finally, diaminobenzidine tetrahydrochloride was implemented to detect signals. According to the intensity of cell staining, negative staining is 0 point, light yellow staining is 1 point, brown-yellow staining is 2 points, and brown staining is 3 points; According to the percentage of positive cells, 1 point is calculated for  $\leq$ 25%, 2 points are calculated for 26% to 50%, 3 points are calculated for 51% to 75%, and 4 points are calculated for  $>$ 75%. The final IHC score is obtained by multiplying the two scores. A total of 21 HGSC patients were enrolled in this study after the informed consent was signed. This study was approved by the ethics committee of Nanjing Women and Children's Healthcare Hospital (No. NFKSL-105).

### Selecting potential therapeutic drugs

To identify potential therapeutic drugs for HGSC patients, the "oncoPredict" R package was used to calculate the correlations between gene expression and the IC50 values of 199 small molecules deposited in the Genomics of Drug Sensitivity in Cancer (GDSC) database ([www.cancerRx-gene.org](http://www.cancerRx-gene.org)).

### Statistical analysis

Statistical analyses were carried out by using GraphPad Prism 8.0 (GraphPad, United States) and R 4.3.0 software. The Wilcoxon test was used to analyze the statistical difference between the 2 groups. The Kaplan-Meier curves with log-rank tests were used to compare the overall survivals of patients between 2 subgroups. The Pearson correlation analysis was applied to calculate the correlations of genes or cell infiltration levels. A  $P$ -value  $<$  .05 was considered statistically significant.

## Results

### Identify CAF-enriched genes based on scRNA-seq data

We first evaluated the infiltration levels of CAFs in HGSC tissues. The TCGA OC cohort showed that the infiltration

levels of CAF were significantly higher in advanced HGSC tumors compared to early ones (Figure 1A). GSE133296 dataset analysis showed that the infiltration levels of CAF were significantly higher in metastatic HGSC compared to primary HGSC (Figure 1B). Consistently, IHC analysis proved that compared to that of HGSC tissues without distant metastasis, the infiltration levels of CAF were significantly elevated in HGSC tissues with distant metastasis (Figure 1C). Subsequently, based on the GSE151214 scRNA-seq dataset, we identified 9 cell types in HGSC tissues, including CAFs (Figure 1D). The presentative markers of each cell type were listed (Figure 1E). Interestingly, the biological process analysis showed that these CAF-enriched genes were significantly associated with cell adhesion, extracellular matrix organization, and positive regulation of cell migration (Figure 1F). The molecular function analysis showed that these genes primarily regulated extracellular matrix structural constituents, fibronectin binding, collagen binding, and integrin binding (Figure 1F). Moreover, the cellular component analysis revealed that the proteins encoded by CAF-enriched genes mainly distributed in the extracellular matrix, extracellular space, and extracellular region (Figure 1F).

### Select CAF-enriched prognostic genes

Subsequently, we selected 42 and 46 CAF-enriched genes that were significantly associated with the patient's prognosis based on the GSE26193 dataset and TCGA HGSC cohort, respectively (Figure 2A and B). Then we overlapped these CAF-enriched prognostic genes and screened 7 common ones, including *TIMP3*, *AXL*, *MFAP4*, *DPT*, *JUN*, *SFRP2*, and *ASPN* (Figure 2C). The distribution of these 7 genes in each cell type was shown in Figure 2D. In addition to *JUN* which was widely expressed in various cell types, the other 6 genes were specifically enriched in CAFs of HGSC tissues. Moreover, CCLE dataset analysis verified that the expression levels of *TIMP3*, *AXL*, *MFAP4*, *DPT*, *JUN*, *SFRP2*, and *ASPN* were significantly upregulated in fibroblasts compared to OC cells (Figure 2E). To further validate the specific distribution of *TIMP3*, *AXL*, *MFAP4*, *DPT*, *JUN*, *SFRP2*, and *ASPN* in CAFs of HGSC tissues, we tested the correlations between their expression levels and CAF infiltrating levels. Based on MCPOUNTER and EPIC algorithms, analyses of the TCGA HGSC cohort and GSE26193 dataset demonstrated that the infiltration levels of CAF were positively correlated with the expression levels of *TIMP3*, *AXL*, *MFAP4*, *DPT*, *JUN*, *SFRP2*, and *ASPN* (Figure 2F and G). Meanwhile, except for *JUN*, the expression levels of *TIMP3*, *AXL*, *MFAP4*, *DPT*, *SFRP2*, and *ASPN* were negatively correlated with tumor purity (Figure 2H).

### Reclassify HGSC patients into distinct subclusters based on CAF-enriched prognostic genes

Subsequently, we reclassified HGSC patients in the GSE26193 dataset into two distinct subclusters based on these

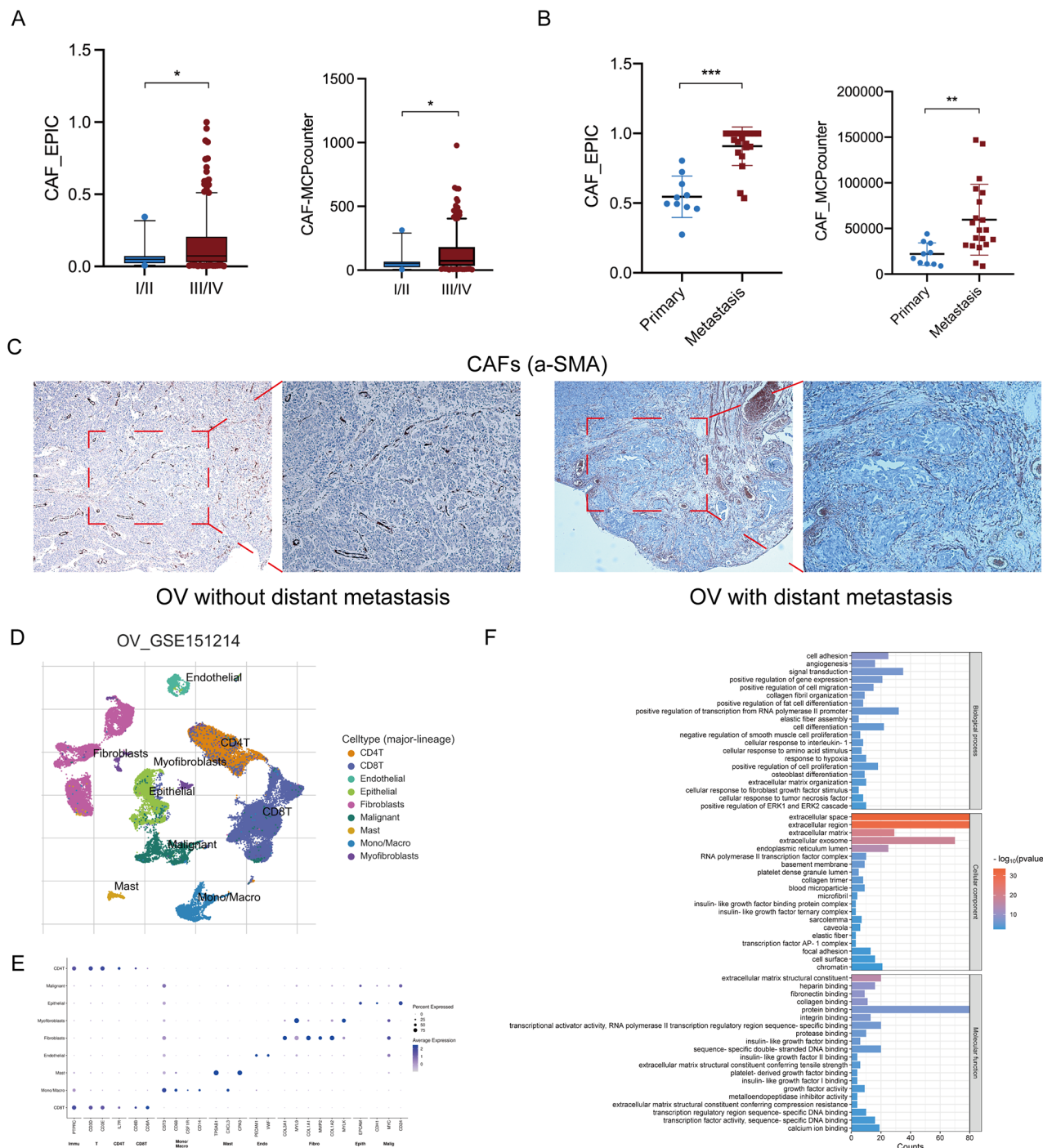


**Figure 1.** Identify CAF-enriched genes based on scRNA-seq analysis: (A) the infiltrated levels of CAFs in advanced and early ovarian carcinoma tissues based on TCGA HGSC cohort, (B) the infiltrated levels of CAFs in primary and metastatic ovarian cancer tissues based on the GSE133296 dataset, (C) IHC analysis of CAFs' infiltrating levels in HGSC tissues with and without distant metastasis, (D) the cell types identified by scRNA-seq based on the GSE151214 dataset, (E) the represented marker genes of each cell type, and (F) GO analysis of genes that were specifically upregulated in CAFs. \* $P < .05$ . \*\* $P < .01$ . \*\*\* $P < .001$ .

CAF-enriched prognostic genes (*TIMP3*, *AXL*, *MEF4*, *DPT*, *SFRP2*, and *ASP1*) by using the Consensus ClusterPlus algorithm (Figure 3A and B). As expected, the stromal scores and CAF infiltrating levels significantly increased in cluster-2 tumor tissues (Figure 3C and D). Besides, the Kaplan-Meier curve analysis showed that HGSC patients in cluster-2 suffered from worse overall survival compared to those in

cluster-1 (HR=2.14, 95% CI: 1.17-3.90,  $P = .0016$ ) (Figure 3E). Moreover, unsupervised clustering analysis of the TCGA HGSC cohort also suggested that HGSC patients were well divided into 2 subclusters (Figure 3F and G). Consistently, the stromal scores and CAF infiltrating levels significantly increased in cluster-2 stromal tissues (Figure 3H and I) and HGSC patients in cluster-2 undergo worse clinical outcomes

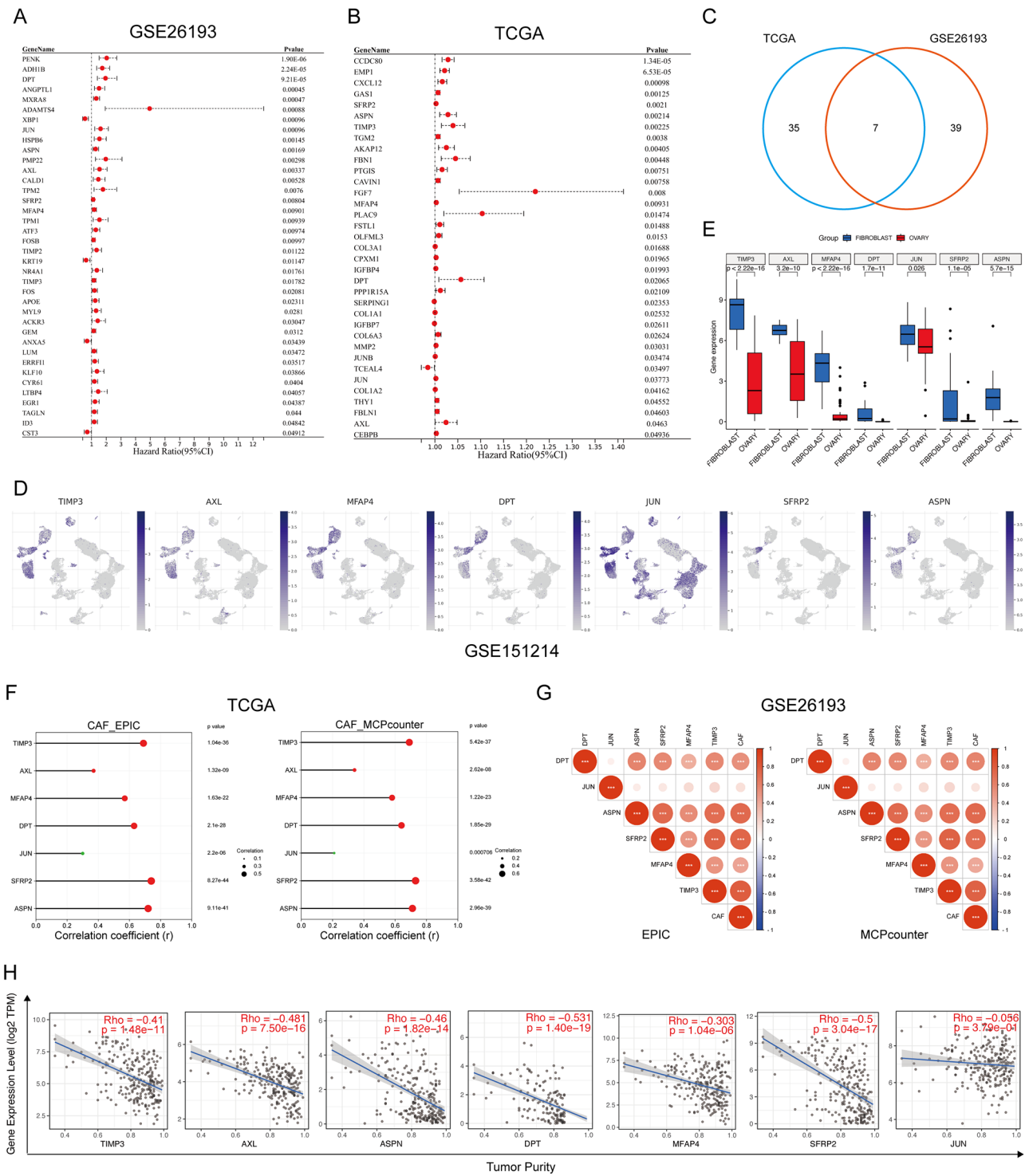


**Figure 2.** Select CAF-enriched prognostic genes: (A) the frost plot of CAF-enriched prognostic genes identified by univariate Cox analysis based on the GSE26193 dataset, (B) the frost plot of CAF-enriched prognostic genes identified by univariate Cox analysis based on the TCGA HGSC cohort, (C) the common CAF-enriched prognostic genes between the GSE26193 dataset and the TCGA HGSC cohort, (D) the distribution of common prognostic CAF-enriched genes in each cell type of HGSC tissues based on the GSE151214 dataset, (E) the expression levels of common prognostic CAF-enriched genes in fibroblasts and ovarian cancer cells based on the CCLE database, (F) the correlations between CAF infiltrating levels and expression levels of *TIMP3*, *AXL*, *MFAP4*, *DPT*, *JUN*, *SFRP2*, and *ASPN* based on the TCGA HGSC cohort, (G) the correlations between CAF infiltrating levels and expression levels of *TIMP3*, *AXL*, *MFAP4*, *DPT*, *JUN*, *SFRP2*, and *ASPN* based on the GSE26193 dataset, and (H) the correlations between tumor purity and expression levels of *TIMP3*, *AXL*, *MFAP4*, *DPT*, *JUN*, *SFRP2*, and *ASPN* based on the TCGA HGSC cohort.

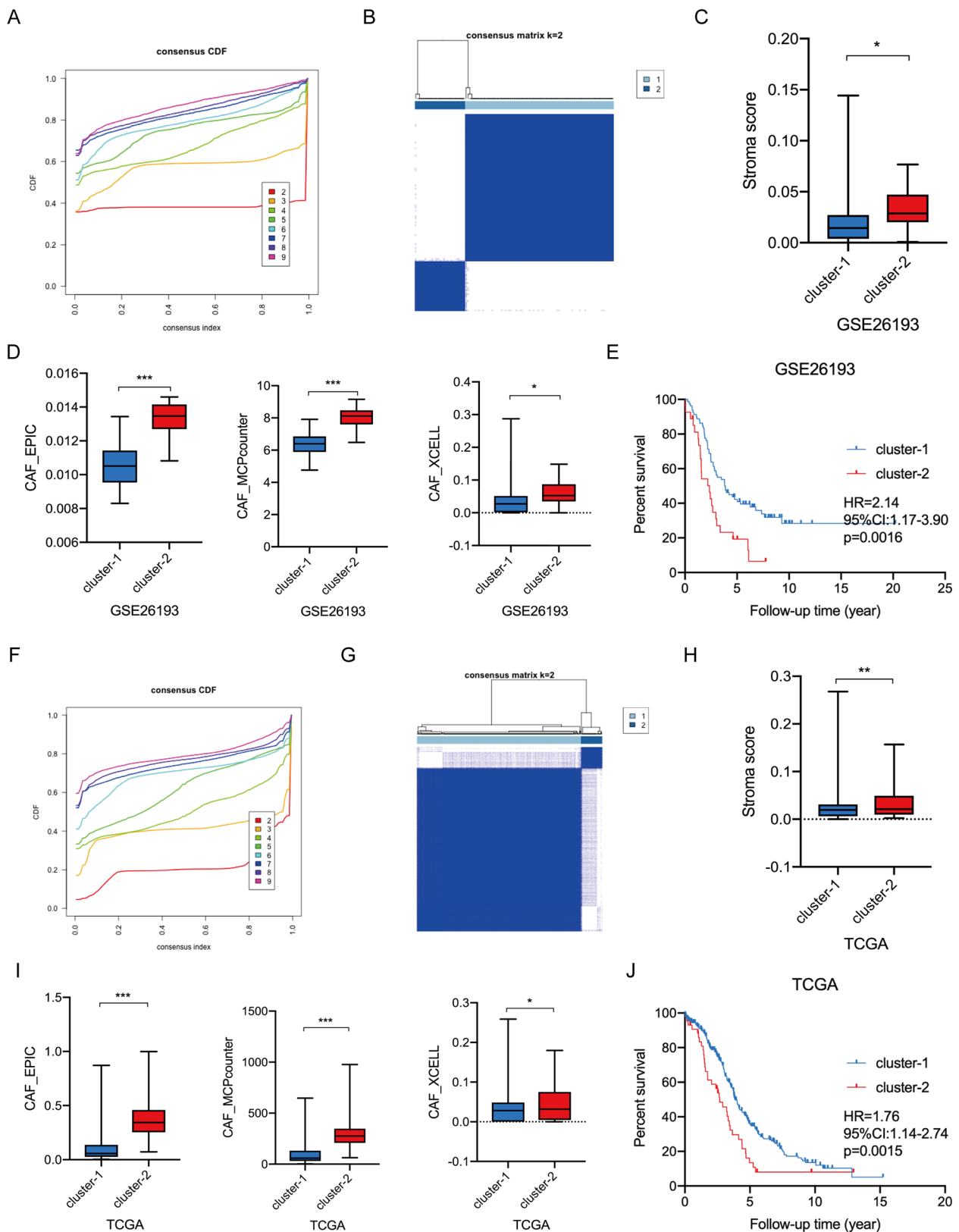


**Figure 3.** Reclassifying HGSC patients into different molecular subtypes based on CAF-enriched prognostic genes: (A) the optimal number of clusters according to the consensus index based on the GSE26193 dataset, (B) consensus clustering analysis of patients according to the consensus index based on the GSE26193 dataset, (C) the stromal scores of cluster-1 and cluster-2 HGSC tissues, (D) the infiltration levels of CAFs between cluster-1 and cluster-2 HGSC tissues, (E) the Kaplan-Meier plot curves of OC patients in cluster-1 and cluster-2 based on the GSE26193 dataset, (F) the optimal number of clusters according to the consensus index based on the GSE26193 dataset, (G) consensus clustering analysis of patients according to the consensus index based on the GSE26193 dataset, (H) the stromal scores of cluster-1 and cluster-2 HGSC tissues, (I) the infiltration levels of CAFs between cluster-1 and cluster-2 HGSC tissues, and (J) the Kaplan-Meier plot curves of OC patients in cluster-1 and cluster-2 based on the GSE26193 dataset.

\* $P < .05$ . \*\* $P < .01$ . \*\*\* $P < .001$ .

**Table 2.** The clinicopathological characteristics of HGSC patients between cluster-1 and cluster-2.

GSE26193		CLUSTER-1	CLUSTER-2	P
FIGO stage	I/II	15	2	
	III/IV	41	21	
Grade	G1/G2	17	6	.13
	G3/G4	39	17	
TCGA		CLUSTER-1	CLUSTER-2	P
Age	<59	163	15	
	≥59	157	27	
FIGO stage	I/II	22	0	
	III/IV	298	42	
Grade	G1/G2	37	6	.064
	G3/G4	283	36	

when compared to cluster-1 HGSC patients (HR=1.76, 95% CI: 1.14-2.74,  $P < .001$ ) (Figure 3J). Moreover, the Chi-square test and Fisher exact test determined that there is no difference in clinicopathological characteristics between cluster-1 patients and cluster-2 patients (Table 2).

#### *The discrepant immunotherapeutic responses of HGSC patients between cluster-1 and cluster-2*

CAFs closely interact with immune cells in the TME.<sup>9</sup> We then investigated the differences in tumor immune microenvironments between cluster-1 and cluster-2 HGSC tissues. Analyses of the TCGA HGSC cohort and GSE26193 dataset demonstrated that the TME and immune scores of cluster-2 tumor tissues were significantly upregulated when compared to those of cluster-1 tumor tissues (Figure 4A and B). In detail, XCELL algorithm analysis revealed that the infiltrated levels of various immune cells, such as macrophage, myeloid dendritic cell activated, monocyte, and CD8+ T cell, significantly increased in cluster-2 HGSC tissues (Figure 4C and D). However, the Tumor Immune Dysfunction and Exclusion (TIDE) scores of cluster-2 tumor tissues were markedly elevated compared to cluster-1 tumor tissues (Figure 4E), indicating that patients in cluster-2 may have difficulty benefiting from immunotherapy. Consistently, the immunophenoscore (IPS) scores further proved that these HGSC patients in cluster-2 were less sensitive to CTLA4 and PD-1 blocker treatment (Figure 4F). Mounting evidence has proved that tumors with higher microsatellite instability (MSI) are more suitable for immunotherapy.<sup>20</sup> Analyses of the TCGA HGSC cohort and GSE26193 dataset both showed that the MSI expression signatures were significantly downregulated in cluster-2 HGSC tissues compared to cluster-1 HGSC tissues (Figure 4G). Moreover, cluster-2 tumor

tissues expressed higher immune checkpoint genes (Figure 4H and I). Overall, these data suggested that although cluster-2 HGSC tissues are “hot” tumors, they are unsuitable for immunotherapy, such as ICI treatment.

#### *The distinct chemotherapeutic responses of HGSC patients between cluster-1 and cluster-2*

At the clinic, platinum and paclitaxel were the typical first-line chemotherapy agents for HGSC patients. To investigate any differences in chemotherapy response between cluster-1 and cluster-2 HGSC, the GSE30161 dataset was analyzed. Based on identified CAF-enriched prognostic genes (*TIMP3*, *AXL*, *MFAP4*, *DPT*, *SFRP2*, and *ASPN*), ovarian adenocarcinomas in this dataset were divided into two subclusters using unsupervised clustering analysis (Figure 5A and B). The MCPCOUNTER and EPIC algorithms, as opposed to the XCELL algorithm, showed that the infiltration levels of CAFs were significantly higher in cluster-2 tumor tissues compared to cluster-1 tumor tissues (Figure 5C). Besides, the Chi-square test indicated that cluster-1 tumor tissues were more likely to be sensitive to adjuvant chemotherapy (Figure 5D). Subsequently, we analyzed 199 compounds to explore potential alternative drugs for cluster-2 tumors based on the GDSC database. Both the TCGA HGSC cohort and GSE26193 dataset results revealed that cluster-2 tumor tissues were more responsive to 24 drug compounds, such as Entospletinib, Cediranib, and Staurosporine (Figure 5E and F).

#### *The specifically enriched gene sets in cluster-2 HGSC tissues*

To explore the molecular difference between cluster-1 and cluster-2 tumor tissues, we conducted a GSEA analysis. GSEA analysis of the TCGA HGSC cohort revealed that the gene sets of EPITHELIAL\_MESENCHYMAL\_TRANSITION, ANGIOGENESIS, COAGULATION, INFLAMMATORY\_RESPONSE, TGF\_BETA\_SIGNALING, IL2\_STAT5\_SIGNALING, TNFA\_SIGNALING\_VIA\_NFKB, COMPLEMENT, HYPOXIA, and APOPTOSIS were significantly enriched in cluster-2 tumor tissues (Figure 6A). The same trend was observed in the GSE26193 dataset (Figure 6B). To further identify gene sets that were specifically enriched in CAFs, we conducted a single-cell GSEA analysis based on the GSE151214 scRNA-seq dataset. We found that two gene sets (EPITHELIAL\_MESENCHYMAL\_TRANSITION and TGF\_BETA\_SIGNALING) were specifically enriched in CAFs (Figure 6C). However, the gene sets of TNFA\_SIGNALING\_VIA\_NFKB, INFLAMMATORY\_RESPONSE, COMPLEMENT, APOPTOSIS, and ANGIOGENESIS were significantly enriched in monocytes/macrophages (Mono/Macro) (Figure 6C). The above results suggested a positive correlation between CAF and Mono/Macro infiltrating levels in HGSC tissues.

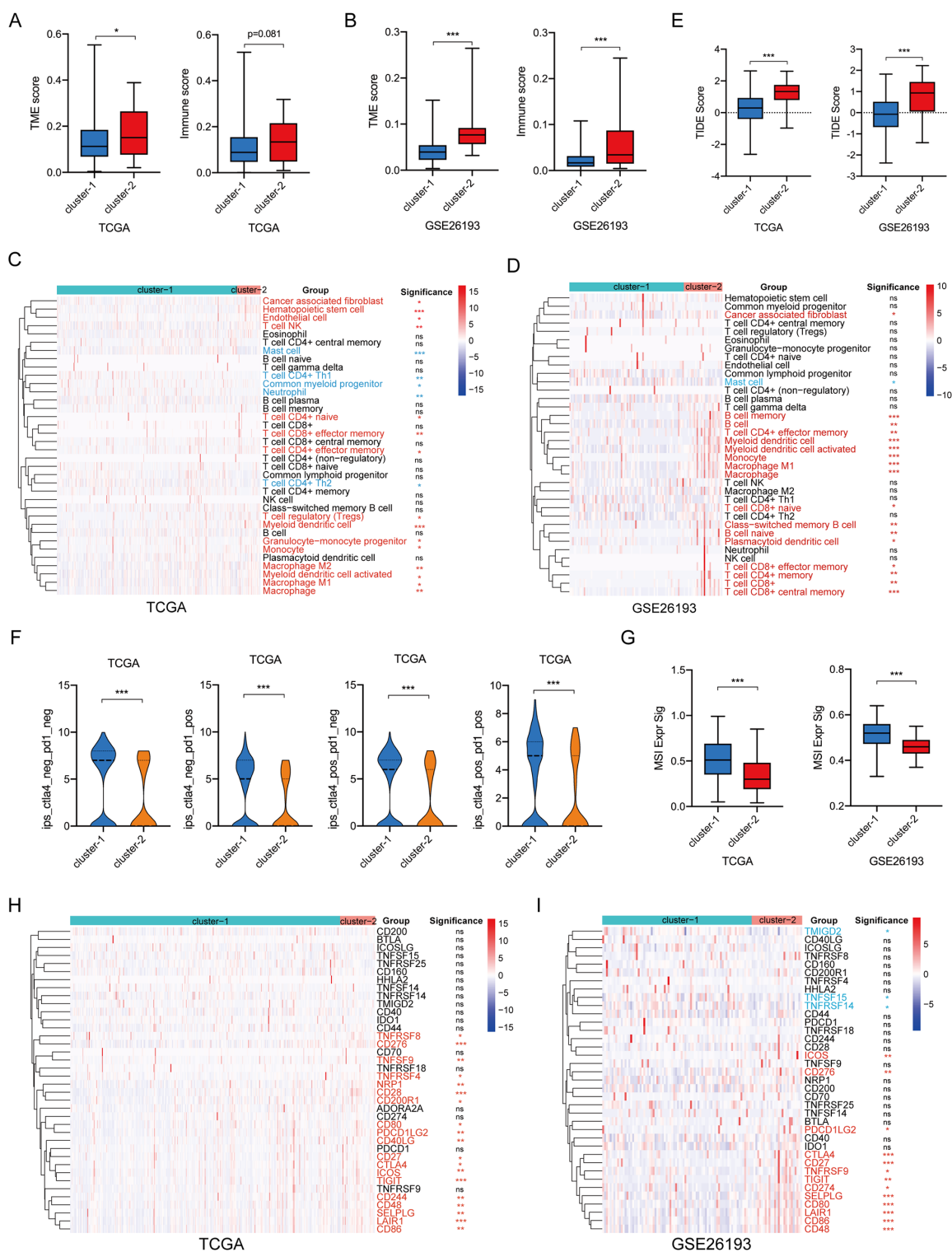


**Figure 4.** The discrepant immunotherapeutic responses of HGSC patients between cluster-1 and cluster-2: (A) the TME scores and immune scores between cluster-1 and cluster-2 based on the TCGA HGSC cohort, (B) the TME scores and immune scores between cluster-1 and cluster-2 based on the GSE26193 dataset, (C) the differentially infiltrated immune cells between cluster-1 and cluster-2 based on the TCGA HGSC cohort, (D) the differentially infiltrated immune cells between cluster-1 and cluster-2 based on the GSE26193 dataset, (E) the TIDE scores between cluster-1 and cluster-2 based on the TCGA HGSC cohort and GSE26193 dataset, (F) the IPS between cluster-1 and cluster-2 based on the TCGA HGSC cohort, (G) the MSI expression signature between cluster-1 and cluster-2 based on the TCGA HGSC cohort and GSE26193 dataset, (H) the differentially expressed immune checkpoint genes between cluster-1 and cluster-2 based on the TCGA HGSC cohort, and (I) the differentially expressed immune checkpoint genes between cluster-1 and cluster-2 based on the GSE26193 dataset.

\* $P < .05$ ; \*\* $P < .01$ ; \*\*\* $P < .001$ ; red, upregulation; blue, downregulation.



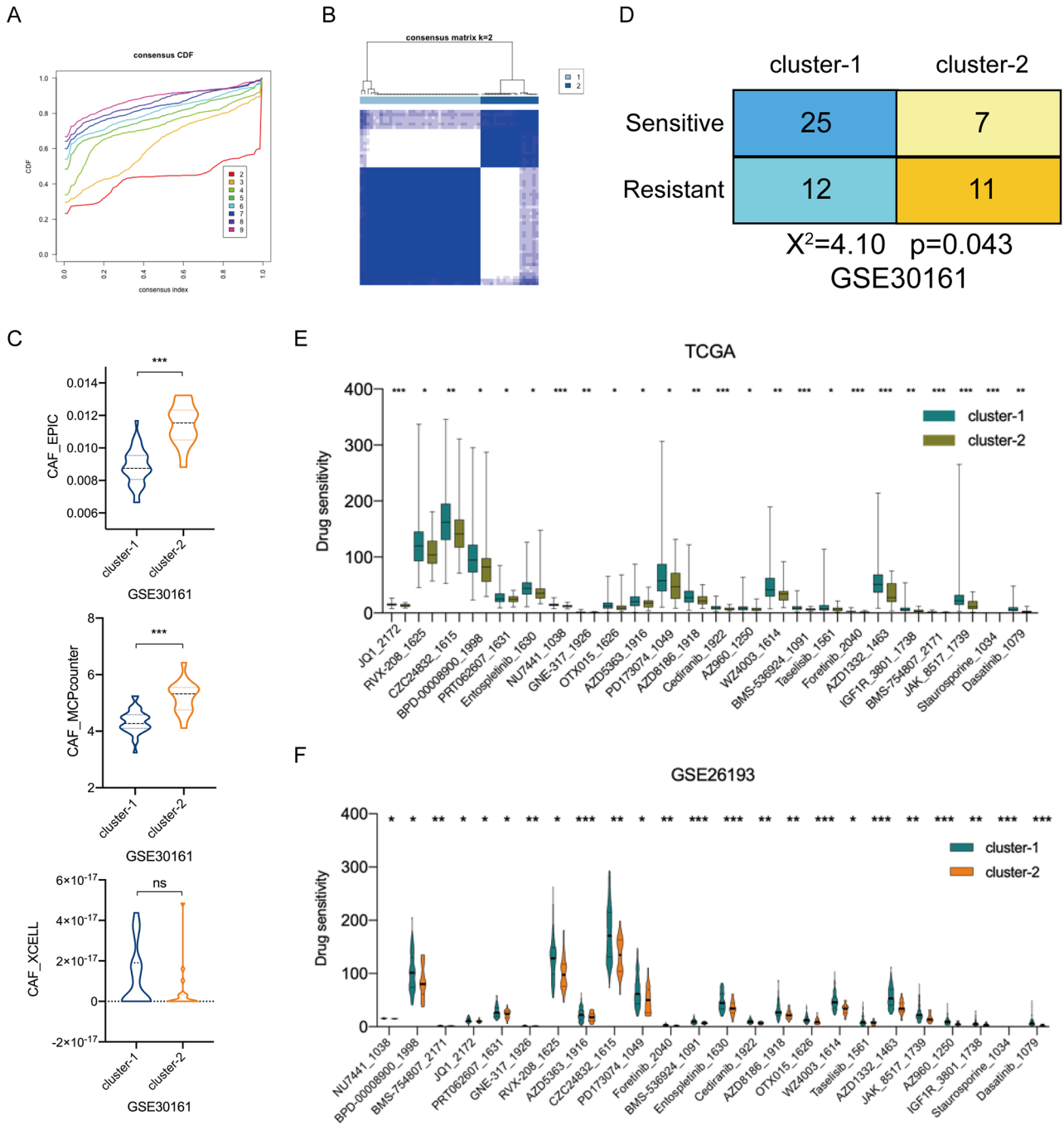


**Figure 5.** Searching for alternative drugs for cluster-2 HGSC patients: (A) the optimal number of clusters according to the consensus index based on the GSE30161 dataset, (B) consensus clustering analysis of patients according to the consensus index based on the GSE30161 dataset, (C) the infiltrated levels of CAFs between cluster-1 and cluster-2, (D) the different response to adjuvant chemotherapy between cluster-1 and cluster-2 revealed by Chi-square test, (E) the alternative drugs for cluster-2 patients based on the TCGA HGSC cohort, and (F) the alternative drugs for cluster-2 HGSC patients based on the GSE26193 dataset. Abbreviation: ns, no significance. \* $P < .05$ . \*\* $P < .01$ . \*\*\* $P < .001$ .

To validate our hypothesis, we analyzed the correlations between CAF markers (*ACTA2*, *FAP*, *COL1A1*, and *FN1*) and Mono/Macro markers (*CD68*, *CD163*, *CD80*, and *MRC1*).<sup>21,22</sup> The results showed that the expression levels of CAF markers were positively correlated with that of Mono/Macro markers in HGSC tissues (Figure 6D and E). Moreover, IHC analysis

directly revealed a positive correlation between CAF and Mono/Macro infiltration levels in HGSC tissues (Figure 6F).

### Discussion

The cancer-related mortality is mainly attributed to metastasis in ovarian carcinoma.<sup>3</sup> It has been proved that CAFs can

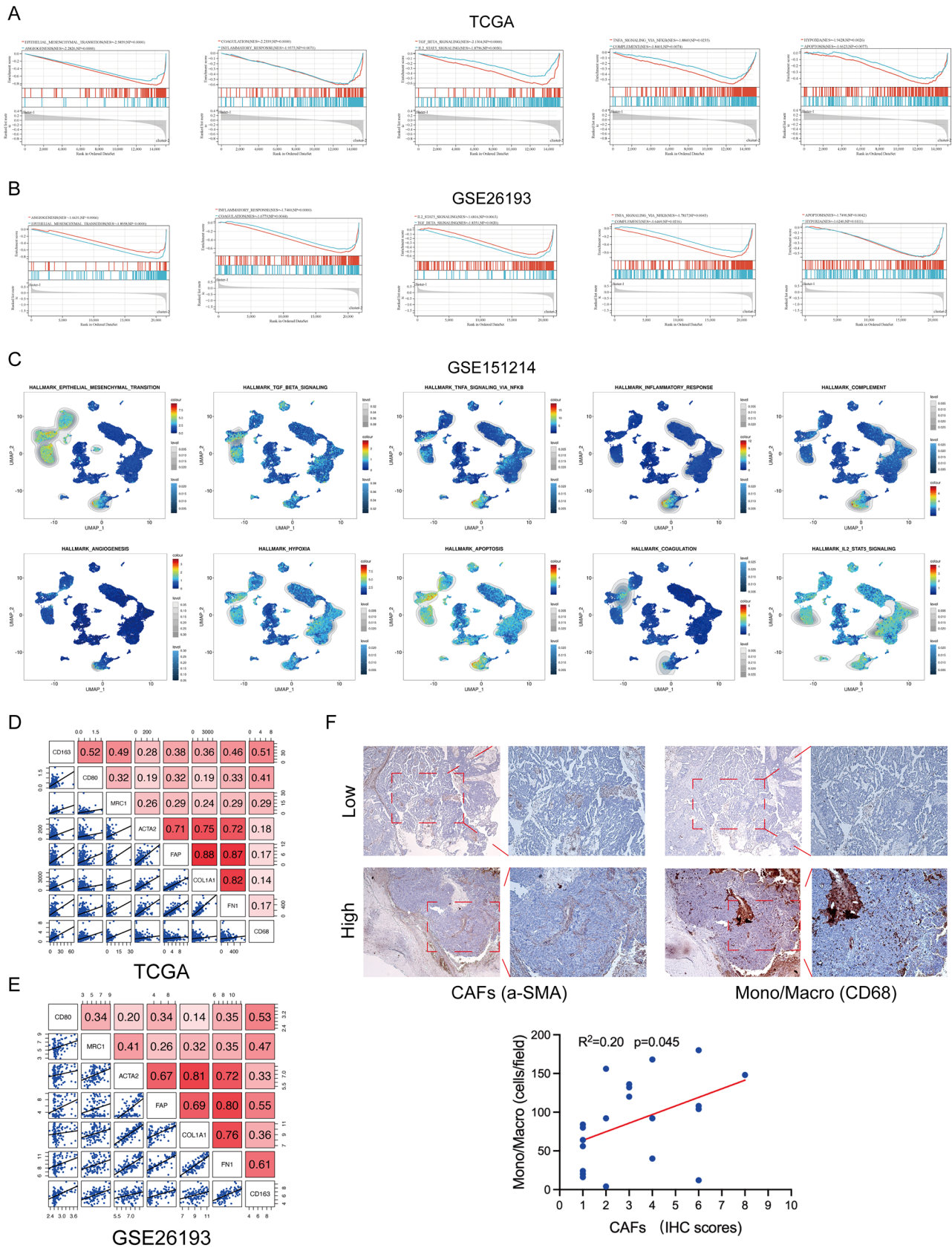


**Figure 6.** The specifically enriched gene sets in cluster-2 tumor tissues: (A) the enriched gene sets of cluster-2 based on the TCGA HGSC cohort, (B) the enriched gene sets of cluster-2 based on the GSE26193 dataset, (C) the specific enriched gene sets in each cell type of HGSC tissues revealed by single-cell GSEA analysis of the GSE151214 dataset, (D) the correlations between CAF markers and Mono/Macro markers based on the TCGA HGSC cohort, (E) the correlations between CAF markers and Mono/Macro markers based on the GSE26193 dataset, and (F) the correlations between CAF infiltrating levels and Mono/Macro infiltrating levels based on IHC analysis of HGSC tissues.

promote tumor metastasis by secreting cytokines, chemokines, extracellular vesicles, metabolites, and remodeling ECM.<sup>23</sup> For example, CAFs inhibit the function of immune cells such as T cells and NK cells by secreting programmed cell death 1 (PD-1), programmed cell death 2 (PD-2), and prostaglandin E2 (PGE2) to facilitate the migration of cancer cells.<sup>24</sup> Consistently, our analysis results revealed that CAFs were significantly elevated in metastatic ovarian carcinoma tissues and were mainly responsible for the reconstruction of surrounding ECM.

The association between patients' prognosis and CAFs infiltration has been widely reported.<sup>25</sup> For instance, CAFs are independent prognostic factors for the survival of non-small cell lung cancer patients.<sup>26</sup> Currently, CAF-associated genes have been applied to predict the prognosis of OC patients.<sup>27,28</sup> Instead, we directly selected HGSC patients with distinct prognoses based on CAF-enriched prognostic genes that were identified by scRNA-seq analysis. We found that *TIMP3*, *AXL*, *MFAP4*, *DPT*, *SFRP2*, and *ASPN* were specifically expressed in CAFs of metastatic HGSC tissues and were significantly associated with the overall survival of patients. *TIMP3* is a prognostic oncogene in OC whose function has been revealed in various cancers.<sup>29,30</sup> Bi et al<sup>31</sup> reported that the MSI1-TIMP3-MMP9 cascade accelerates breast carcinoma metastasis by regulating extracellular matrix degradation. *AXL* is an essential therapeutic target for metastatic OC.<sup>32</sup> Mullen et al<sup>33</sup> reported that inhibiting *AXL* enhances the sensitivity of ovarian carcinoma to chemotherapy and PARP inhibition treatment. *MFAP4* affects elastic fiber homeostasis, integrin signaling, and cancer progression.<sup>34</sup> High *MFAP4* expression could predict platinum-based chemoresistance in serous OC patients.<sup>35</sup> *DPT* was reported to play an anti-proliferative role in breast cancer.<sup>36</sup> However, its role in ovarian cancer has not been investigated. Our results revealed that *DPT* was specifically enriched in CAFs and inversely correlated with the prognosis of HGSC patients. Therefore, we hypothesized that DPT + CAFs may promote HGSC malignancy progression. *SFRP2* is an upstream antagonist of canonical Wnt/ $\beta$ -catenin signaling and promotes the epithelial-mesenchymal transition of OC cells.<sup>37</sup> Our data identified that *ASPN* was specifically distributed in CAFs of HGSC tissues. Consistently, an *ASPN*<sup>high</sup> CAF population that is located at the distal invading front was identified in gastric carcinoma.<sup>38</sup> *JUN* is a transcription factor that recognizes and binds to the AP-1 consensus motif.<sup>39</sup> The oncogenic role of *JUN* has been validated in OC.<sup>40</sup> However, our scRNA-seq analysis results showed that all types of cells express *JUN* in HGSC tissues, which indicated that *JUN* is essential for cell survival. We had to admit that this is an in silico study and the expression and function of these genes ought to be experimentally validated in subsequent studies.

Accumulating investigations found that tumor-associated macrophages are the most prominent immune cells in the vicinity of CAF-populated areas, indicating a tight interaction between these 2 cell types.<sup>41</sup> In the present study, we discovered

that the infiltrated levels of CAFs are positively correlated with that of monocytes/macrophages in ovarian cancer tissues. Many studies have proved that CAFs enhance the recruitment and M2-type differentiation of macrophages (pro-tumorigenic subsets) to impair responses from effector T cells and induce immune suppression microenvironment.<sup>42</sup> In the present study, we uncovered that HGSC tissues in cluster-2 with higher infiltrated CAFs owned more infiltrated immune cells, but responded worse to immunotherapy, such as CTLA4 blocker and PD-1 blocker. TGF- $\beta$ 1 + CAFs were reported to determine the efficacy of immunotherapy<sup>43</sup> and targeting CAF differentiation could overcome immunotherapy resistance.<sup>44</sup> Consistently, our GSEA analysis results demonstrated that the gene set of TGF- $\beta$  signaling was significantly enriched in CAFs whose infiltration levels were markedly upregulated in cluster-2 HGSC tissues. In addition, our study discovered that these HGSC patients in cluster-2 were also more likely to be resistant to traditional chemotherapy. Deying et al<sup>11</sup> reported that CAF-derived HGF promotes ovarian carcinoma cell proliferation and drug resistance via the c-Met/PI3K/AKT and GRP78 signal. What is noteworthy is that, with the development of scRNA-seq technology, CAFs were found to consist of various subtypes. Therefore, targeting CAF subtypes responsible for specific tumor phenotypes is a promising therapeutic strategy for OC patients. Furthermore, we selected 24 drug compounds, such as Entospletinib and Cediranib, as the potential alternative to traditional treatment of ovarian carcinoma patients. Currently, the combination of Entospletinib and traditional chemotherapy has been investigated in chronic and acute lymphocytic leukemia.<sup>45,46</sup> Cediranib has been widely used in OC as monotherapy and in combination with chemotherapy, PARP inhibitors, and immunotherapy.<sup>47</sup> For example, compared with chemotherapy, a combination of olaparib/cediranib improves the progression-free survival of OC patients with a germline BRCA mutation and results in reduced patient-reported outcomes.<sup>48</sup> *TP53*, *BRCA1*, and *BECN1* are 3 tumor suppressor genes that are frequently deleted, silenced, or mutated in OC and are significantly associated with drug-resistance.<sup>49</sup> Therefore, the combination of *TP53*, *BRCA1*, and *BECN1* status and CAFs-enriched genes may improve the predictive ability of therapeutic response.

In conclusion, our study reclassified HGSC patients into 2 molecular subtypes with distinct prognoses and discrepant responses to chemotherapy and immunotherapy based on CAF-enriched prognostic genes. In addition, we further verified the close cross-talk between CAFs and macrophages in TME.

### Author Contributions

All authors contributed to the study's conception and design. Material preparation, data collection, and analysis were performed by Xiangxiang Liu, Guoqiang Ping, and Dongze Ji. The first draft of the manuscript was written by Zhifa Wen

and Yajun Chen commented on previous versions of the manuscript. All authors read and approved the final manuscript.

### Data Availability Statement

The datasets generated during and/or analyzed during the current study are available from the corresponding author upon reasonable request.

### Ethics Approval

This study was performed in line with the principles of the World Medical Association Declaration of Helsinki. Approval was granted by the Ethics Committee of Women's Hospital of Nanjing Medical University (No. NFKSL-105).

### ORCID iD

Yajun Chen  <https://orcid.org/0009-0007-1983-1997>

### REFERENCES

- Morand S, Devanaboyina M, Staats H, Stanbery L, Nemunaitis J. Ovarian cancer immunotherapy and personalized medicine. *Int J Mol Sci.* 2021;22:6532.
- Lliberos C, Richardson G, Papa A. Oncogenic pathways and targeted therapies in ovarian cancer. *Biomolecules.* 2024;14:585.
- Yousefi M, Dehghani S, Nosrati R, et al. Current insights into the metastasis of epithelial ovarian cancer - hopes and hurdles. *Cell Oncol.* 2020;43:515-538.
- Miyamoto T, Murphy B, Zhang N. Intraperitoneal metastasis of ovarian cancer: new insights on resident macrophages in the peritoneal cavity. *Front Immunol.* 2023;14:1104694.
- Shi X, Yu X, Wang J, et al. SIK2 promotes ovarian cancer cell motility and metastasis by phosphorylating MYLK. *Mol Oncol.* 2022;16:2558-2574.
- de Visser KE, Joyce JA. The evolving tumor microenvironment: from cancer initiation to metastatic outgrowth. *Cancer Cell.* 2023;41:374-403.
- Gao Q, Yang Z, Xu S, et al. Heterotypic CAF-tumor spheroids promote early peritoneal metastasis of ovarian cancer. *J Exp Med.* 2019;216:688-703.
- Sun L, Ke M, Wang X, et al. FAP(high)  $\alpha$ -SMA(low) cancer-associated fibroblast-derived SLPI protein encapsulated in extracellular vesicles promotes ovarian cancer development via activation of PI3K/AKT and downstream signaling pathways. *Mol Carcinog.* 2022;61:910-923.
- Mao X, Xu J, Wang W, et al. Crosstalk between cancer-associated fibroblasts and immune cells in the tumor microenvironment: new findings and future perspectives. *Mol Cancer.* 2021;20:131.
- Zhang A, Qian Y, Ye Z, et al. Cancer-associated fibroblasts promote M2 polarization of macrophages in pancreatic ductal adenocarcinoma. *Cancer Med.* 2017;6:463-470.
- Deying W, Feng G, Shumei L, et al. CAF-derived HGF promotes cell proliferation and drug resistance by up-regulating the c-Met/PI3K/Akt and GRP78 signalling in ovarian cancer cells. *Biosci Rep.* 2017;37:BSR20160470.
- Chu L, Wang F, Zhang W, et al. Periostin secreted by carcinoma-associated fibroblasts promotes ovarian cancer cell platinum resistance through the PI3K/Akt signaling pathway. *Technol Cancer Res Treat.* 2020;19:1533033820977535.
- Sulaiman R, De P, Aske JC, et al. Patient-derived primary cancer-associated fibroblasts mediate resistance to anti-angiogenic drug in ovarian cancers. *Bio-medicines.* 2023;11:112.
- Zhao Y, Mei S, Huang Y, et al. Integrative analysis deciphers the heterogeneity of cancer-associated fibroblast and implications on clinical outcomes in ovarian cancers. *Comput Struct Biotechnol J.* 2022;20:6403-6411.
- Hu Y, Taylor-Harding B, Raz Y, et al. Are epithelial ovarian cancers of the mesenchymal subtype actually intraperitoneal metastases to the ovary? *Front Cell Dev Biol.* 2020;8:647.
- Gentric G, Kieffer Y, Mieulet V, et al. PML-regulated mitochondrial metabolism enhances chemosensitivity in human ovarian cancers. *Cell Metab.* 2019;29:156-173.e10.
- Ferriss JS, Kim Y, Duska L, et al. Multi-gene expression predictors of single drug responses to adjuvant chemotherapy in ovarian carcinoma: predicting platinum resistance. *PLoS One.* 2012;7:e30550.
- Dinh HQ, Lin X, Abbasi F, et al. Single-cell transcriptomics identifies gene expression networks driving differentiation and tumorigenesis in the human fallopian tube. *Cell Rep.* 2021;35:108978.
- Sun D, Wang J, Han Y, et al. TISCH: a comprehensive web resource enabling interactive single-cell transcriptome visualization of tumor microenvironment. *Nucleic Acids Res.* 2020;49:D1420-d1430.
- Coutzac C, Bibeau F, Ben Abdelghani M, et al. Immunotherapy in MSI/dMMR tumors in the perioperative setting: the IMHOTEP trial. *Dig Liver Dis.* 2022;54:1335-1341.
- Nurmik M, Ullmann P, Rodriguez F, Haan S, Letellier E. In search of definitions: cancer-associated fibroblasts and their markers. *Int J Cancer.* 2020;146:895-905.
- Jablonski KA, Amici SA, Webb LM, et al. Novel markers to delineate murine M1 and M2 macrophages. *PLoS One.* 2015;10:e0145342.
- Walker C, Mojares E, Del Río Hernández A. Role of extracellular matrix in development and cancer progression. *Int J Mol Sci.* 2018;19:3028.
- Li C, Teixeira AF, Zhu HJ, Ten Dijke P. Cancer associated-fibroblast-derived exosomes in cancer progression. *Mol Cancer.* 2021;20:154.
- Ren Q, Zhang P, Zhang X, et al. A fibroblast-associated signature predicts prognosis and immunotherapy in esophageal squamous cell cancer. *Front Immunol.* 2023;14:1199040.
- Cords L, Engler S, Haberecker M, et al. Cancer-associated fibroblast phenotypes are associated with patient outcome in non-small cell lung cancer. *Cancer Cell.* 2024;42:396-412.e5.
- Zeng L, Wang X, Wang F, Zhao X, Ding Y. Identification of a gene signature of cancer-associated fibroblasts to predict prognosis in ovarian cancer. *Front Genet.* 2022;13:925231.
- Feng S, Xu Y, Dai Z, et al. Integrative analysis from multicenter studies identifies a WGCNA-derived cancer-associated fibroblast signature for ovarian cancer. *Front Immunol.* 2022;13:951582.
- Chang RM, Fu Y, Zeng J, Zhu XY, Gao Y. Cancer-derived exosomal miR-197-3p confers angiogenesis via targeting TIMP2/3 in lung adenocarcinoma metastasis. *Cell Death Dis.* 2022;13:1032.
- Zhou Y, Zhang T, Wang S, et al. Targeting of HBP1/TIMP3 axis as a novel strategy against breast cancer. *Pharmacol Res.* 2023;194:106848.
- Bi X, Lou P, Song Y, et al. Msi1 promotes breast cancer metastasis by regulating invadopodia-mediated extracellular matrix degradation via the timp3-mmp9 pathway. *Oncogene.* 2021;40:4832-4845.
- Rankin EB, Fuh KC, Taylor TE, et al. AXL is an essential factor and therapeutic target for metastatic ovarian cancer. *Cancer Res.* 2010;70:7570-7579.
- Mullen MM, Lomonosova E, Toboni MD, et al. GAS6/AXL inhibition enhances ovarian cancer sensitivity to chemotherapy and PARP inhibition through increased DNA damage and enhanced replication stress. *Mol Cancer Res.* 2022;20:265-279.
- Mohammadi A, Sorensen GL, Pilecki B. MFAP4-mediated effects in elastic fiber homeostasis, integrin signaling and cancer, and its role in teleost fish. *Cells.* 2022;11:2115.
- Zhao H, Sun Q, Li L, et al. High expression levels of AGGF1 and MFAP4 predict primary platinum-based chemoresistance and are associated with adverse prognosis in patients with serous ovarian cancer. *J Cancer.* 2019;10:397-407.
- Su Y, Du Y, Ye S, et al. Clinical importance and PI3K/Akt pathway-dependent anti-proliferative role of PALMD and DPT in breast cancer. *Pathol Res Pract.* 2023;249:154717.
- Duan H, Yan Z, Chen W, et al. TET1 inhibits EMT of ovarian cancer cells through activating Wnt/ $\beta$ -catenin signaling inhibitors DKK1 and SFRP2. *Gynecol Oncol.* 2017;147:408-417.
- Itoh G, Takagane K, Fukushi Y, et al. Cancer-associated fibroblasts educate normal fibroblasts to facilitate cancer cell spreading and T-cell suppression. *Mol Oncol.* 2022;16:166-187.
- Qing J, Zhang Y, Derynck R. Structural and functional characterization of the transforming growth factor- $\beta$ -induced Smad3/c-jun transcriptional cooperativity. *J Biol Chem.* 2000;275:38802-38812.
- Xiaohua ZHU, Xie Y, Huang W, Chen Z, Guo S. NAP1L1 promotes tumor proliferation through HDGF/C-JUN signaling in ovarian cancer. *BMC Cancer.* 2022;22:339.
- Herrera M, Herrera A, Domínguez G, et al. Cancer-associated fibroblast and M2 macrophage markers together predict outcome in colorectal cancer patients. *Cancer Sci.* 2013;104:437-444.
- Tan B, Shi X, Zhang J, et al. Inhibition of rspo-1gr4 facilitates checkpoint blockade therapy by switching macrophage polarization. *Cancer Res.* 2018;78:4929-4942.
- Vienot A, Pallandre JR, Renaude E, et al. Chemokine switch regulated by TGF- $\beta$ 1 in cancer-associated fibroblast subsets determines the efficacy of chem-immunotherapy. *OncImmunology.* 2022;11:2144669.
- Mellone M, Piotrowska K, Venturi G, et al. ATM regulates differentiation of myofibroblastic cancer-associated fibroblasts and can be targeted to overcome immunotherapy resistance. *Cancer Res.* 2022;82:4571-4585.

45. Sharman J, Di Paolo J. Targeting B-cell receptor signaling kinases in chronic lymphocytic leukemia: the promise of entospletinib. *Ther Adv Hematol*. 2016;7:157-170.
46. Loftus JP, Yahiaoui A, Brown PA, et al. Combinatorial efficacy of entospletinib and chemotherapy in patient-derived xenograft models of infant acute lymphoblastic leukemia. *Haematologica*. 2021;106:1067-1078.
47. Orbegoso C, Marquina G, George A, Banerjee S. The role of cediranib in ovarian cancer. *Expert Opin Pharmacother*. 2017;18:1637-1648.
48. Liu JF, Brady MF, Matulonis UA, et al. Olaparib with or without cediranib versus platinum-based chemotherapy in recurrent platinum-sensitive ovarian cancer (NRG-GY004): a randomized, open-label, phase III trial. *J Clin Oncol*. 2022;40:2138-2147.
49. Salwa A, Ferraresi A, Chinthakindi M, et al. BECN1 and BRCA1 deficiency sensitizes ovarian cancer to platinum therapy and confers better prognosis. *Bio-medicines*. 2021;9:207.